Journal of Nepal Geological Society, 2024, Vol. 67, pp. 49–58
https://doi.org/10.3126/jngs.v67i1.74583

High-frequency coda wave attenuation in the Mid and Far-Western region of the Nepal Himalaya

***Thakur Prasad Kandel, Gautam Prashad Khanal and Krishna Pandey**

Department of Mines and Geology, Ministry of Industry, Commerce and Supplies, Government of Nepal
**Corresponding author's email: thakurkndl@gmail.com*

ABSTRACT

In this study, we utilized the vertical components seismograms of 111 local earthquakes (Ml 2.5-5.5) recorded at fourteen stations by the HiKNet network, to present the first-ever estimate of the high-frequency coda waves attenuation in the Mid and Far-Western region of Nepal Himalaya. The inverse of coda wave attenuation, Q_c (quality factor) is estimated at eight central frequencies of 1.5, 3.0, 6.0, 9.0, 12.0, 15.0, 18.0, and 21.0 Hz through 30 s coda window length by using the single back-scattering model. Our findings are expressed in terms of the (Q_c) quality factor, showing a clear frequency-dependent power relation, $Q_c(f) = Q_0 f^n$ where Q_0 is Q_c at 1 Hz, f is the frequency and n represents the degree of frequency dependence. The estimated average quality factor (Intrinsic and scattering quality factor) of all these seismic stations was obtained as $(91.8 \pm 7.3) f^{1.07 \pm 0.03}$ at 30 s coda window length, which represents the highly heterogeneous and seismo-tectonically active region. The relatively lower quality factor (Q_c) value was obtained around Bajhang compared to the Mugu and Dailekh seismic belts. The Q_0 and n obtained in this study are consistent with previous research in the Central Region of the Nepal Himalaya and results with similar tectonic settings from other seismically active regions.

Keywords: Coda wave; Attenuation; Coda Q; Single back-scattering model.

Received: 6 May 2024 **Accepted:** 26 September 2024

INTRODUCTION

Coda wave, also known as scattered wave, is a type of seismic wave generated by the scattering of seismic energy as it propagates through the heterogeneous medium. According to Aki (1969) and Aki and Chouet (1975), coda waves are not direct waves coming from an earthquake source but are back-scattered waves generated due to the presence of medium heterogeneities that appear after the arrival of body wave, coming after direct S wave and can be identified as S coda wave or simply coda waves (Aki and Chouet, 1975; Sato, 1977a). It is found that for the coda waves of the local earthquakes, whose hypocenter is less than twice the Moho depth (less than 100 Km in Nepal Himalaya), their power spectra, and coda duration are relatively independent of focal distance (Aki and Chouet, 1975). So the coda wave attenuation is frequency-dependent (Dainty, 1981) in the 1 to 20 Hz frequency range.

The energy of seismic waves decreases during propagation through media due to various phenomena such as geometric dispersion, scattering, and intrinsic attenuation (Aki and Chouet, 1975; Stein and Wysession, 2009). Geometric propagation is the decrease in seismic wave amplitude due to spherical expansion of the wavefront (Sato and Fehler, 1998) and is dependent on hypocentral distance. On the other hand, intrinsic absorption is mostly controlled by thermal conditions (Aki, 1980; Havskov et al., 1989; Canas et al., 1995; Stein and Wysession, 2009; Yavuz and Baris, 2019) of the medium. Similarly, scattering reduces the seismic energy and is directly related to media heterogeneity. Seismic wave attenuation is a dimensionless quantity, expressed as the reciprocal of the quality factor (Q^{-1}) (Aki and Chouet, 1975). The mathematical distinction between intrinsic and scattering attenuation is not a simple task (Sato et al., 2012), but for practical use, there is often no need to separate intrinsic and scattering attenuation, as it is usually the total attenuation that is of interest (Havskov and Ottemoller, 2010).

Among the different techniques used, the single back-scattering model of Aki and Chouet (1975) and the single isotropic scattering models of Sato (1977b) are the most popular. The single back-scattering method is valid for signals that arrive long after the primary waves, as it is based on the assumption that the coda waves amplitude should decrease with lapse time at a particular frequency due to seismic energy attenuation, and are not influenced by factors such as earthquake source characteristics, path effects, or site amplification, as discussed by Aki (1969).

The study of coda wave attenuation provides valuable information about the region's medium heterogeneity and attenuation characteristics. The attenuation of coda waves is widely studied in different tectonic settings of the world. However, despite having a wealth of seismic data, the Mid and Far-Western Nepal Himalaya is still overlooked in terms of seismic wave attenuation studies. Limited seismological studies (Pandey et al., 1999; Hossler et al., 2016; Hoste-colomer et al., 2018; Subedi et al., 2018; Laporte et al., 2021; Riesner et al., 2021) have been carried out beneath the Mid and the Far-Western regions to explore the tectonic evolution, historical earthquakes and geometrical fault structure beneath it. In this work, we used the single back-scattering method of

Aki and Chouet (1975) to understand the coda wave attenuation in the Mid and Far-Western regions of the Nepal Himalaya at eight different central frequencies at 30 s coda window length (Table 1). The study will enhance knowledge on regional coda wave attenuation characteristics and provide insight into the quantitative evaluation of earthquake ground motion of the seismo-tectonically active region.

GEOLOGY AND SEISMOTECTONIC

The Mid and Far-Western region of the Nepal Himalaya lies at the central part of the Himalayan arc, which results from the active continent-continent collision between the northward-moving Indian plate and the Eurasian plate (Molnar and Tapponnier, 1975). This convergence process is still continuous at an average rate of about 20.02 mm/y in the Nepal Himalaya (Stevens and Avouac, 2015; Tabei et al., 2024). Due to active crustal shortening, the probability of earthquake occurrence around the Nepal Himalaya is very high and most of these earthquakes occur at shallow depths and interplate.

The study area consists of parts of the Siwalik, the Lesser Himalaya and the Higher Himalaya, and Tethys Himalaya units, which are thrust along the North dipping crustal thrust systems, the Main Frontal Thrust (MFT), the Main Boundary Thrust (MBT), and the Main Central Thrust (MCT) (DMG, 2020) from south to north (Fig. 1). Dadeldhura Klippe and Karnali Klippe (thrust part of the Higher Himalaya) are the major geological structures within our study area. The lower part of the Dadeldhura Klippe consists of grey-green garnet schists, quartzites, and gneisses (Dhital, 2015), while the syn-formal Karnali Klippe consists of mainly gneisses. The seismic stations and events used in the study are located in the Lesser Himalaya (the Kuncha Group and the Nawakot Group) and Higher Himalaya (Fig. 1). The Higher Himalaya consists of high-grade metamorphic rocks (garnet schists, quartzite, gneisses) sandwiched between the sedimentary sequence (Limestone, sandstone, and shales) of the Tethys Himalaya and meta-sedimentary sequence of the Lesser Himalaya (phyllites, quartzites, and carbonates). The crustal thrusts MFT, MBT, and MCT are considered rooted as to depth in a low angle decollement, called Main Himalaya Thrust (MHT), which produces most of the crustal deformation in the Himalaya (Cattin and Avouac, 2000).

Table 1: Different central frequency components of Butterworth bandpass filter with low and high cutoff frequencies in Hz.

Low Cutoff	Central Frequency (Hz)	High Cutoff
1	1.5	2
2	3	4
4.5	6	7.5
6	9	12
8	12	16
10	15	20
12	18	24
14	21	28

The Mid and Far-Western region is a seismo-tectonically active zone based on microseismic events. Six moderate earthquakes (between 6 - 7 Ml) have been reported in this region since instrumentation in Nepal (Fig. 1). Among them, the Bajhang and Jajarkot earthquakes are the latest moderate earthquakes that occurred in 2023 within one month. Despite being seismically active, the region stands as a seismic gap in terms of large earthquakes (Pandey et al., 1999) when compared with Central Nepal where frequent large earthquakes greater than Mw 7.5 have occurred (Bilham, 1995; Pandey et al., 1999). Noteworthy, microseismicity in the study area shows significant lateral variation (Pandey et al., 1999; Hoste-colomer et al., 2018; Laporte et al., 2021). The Far-Western region has denser seismicity around the Bajhang area (Pandey et al., 1999) as compared to the Dailekh and Mugu areas (Hoste-colomer et al., 2018), probably due to the segmentation of the Main Himalayan Thrust Fault (Pandey et al., 1999). Based on the microseismicity, the study area can be divided into three seismic zones Bajhang, Mugu, and Dailekh Siesmic belts, and is partially controlled by geological structures (Pandey et al., 1999; Hoste-colomer et al., 2018; Laporte et al., 2021).

DATA ACQUISITION

We have used 111 well-located local earthquakes of magnitude ranges between 2.5 to 5.5 Ml, and focal depth up to 25 Km, from the HiKNet network (Himalayan-Karnali network), using the earthquake catalog of Hoste-colomer et al. (2018) recorded from December 2014 to November 2015, by fourteen seismometers. The Himalaya Karnali Network was a temporary seismic network, deployed from November 2014 to September 2016 through Western Nepal (Hoste-colomer et al., 2018; Laporte et al., 2021). The network consisted of 15 seismic stations, composed of 8 Guralp CMG40 and 7 Lennartz Le3D5s seismometers with Nanometrics Taurus digitizers provided by the French mobile instruments RESIF- SISMOB, distributed in 3 sub-arrays (Hoste-colomer et al., 2018).

Only vertical components seismograms of each selected event (sampling frequency 100 Hz) were used in this study. Raw seismic data from the HiKNet stations are in open access through the RESIF web service (Bollinger et al., 2011). After downloading the waveform data, a Seismic Analysis Code (Goldstein and Snoke, 2005) was used to select the individual station's seismograms. Only good-quality waveforms (free from contamination of other events, and counterfeit signals) have been selected for further analysis. Downloaded waveforms of individual seismic stations were also filtered out based on hypocentre distance between 15-100 Km. Most of the events are concentrated around the seismic stations (Fig. 1). Stations were installed close to the bedrock, relatively far from local noise sources, and seismic stations were installed around the Bajhang, Mugu, and Dailekh seismic belts (Fig.1).

METHODOLOGY AND DATA ANALYSIS

Different methods used to determine the attenuation characteristics of coda waves include single back-scattering, multiple scattering, stacking and averaging, spectral ratio, and empirical methods. The single back-scattering model remains

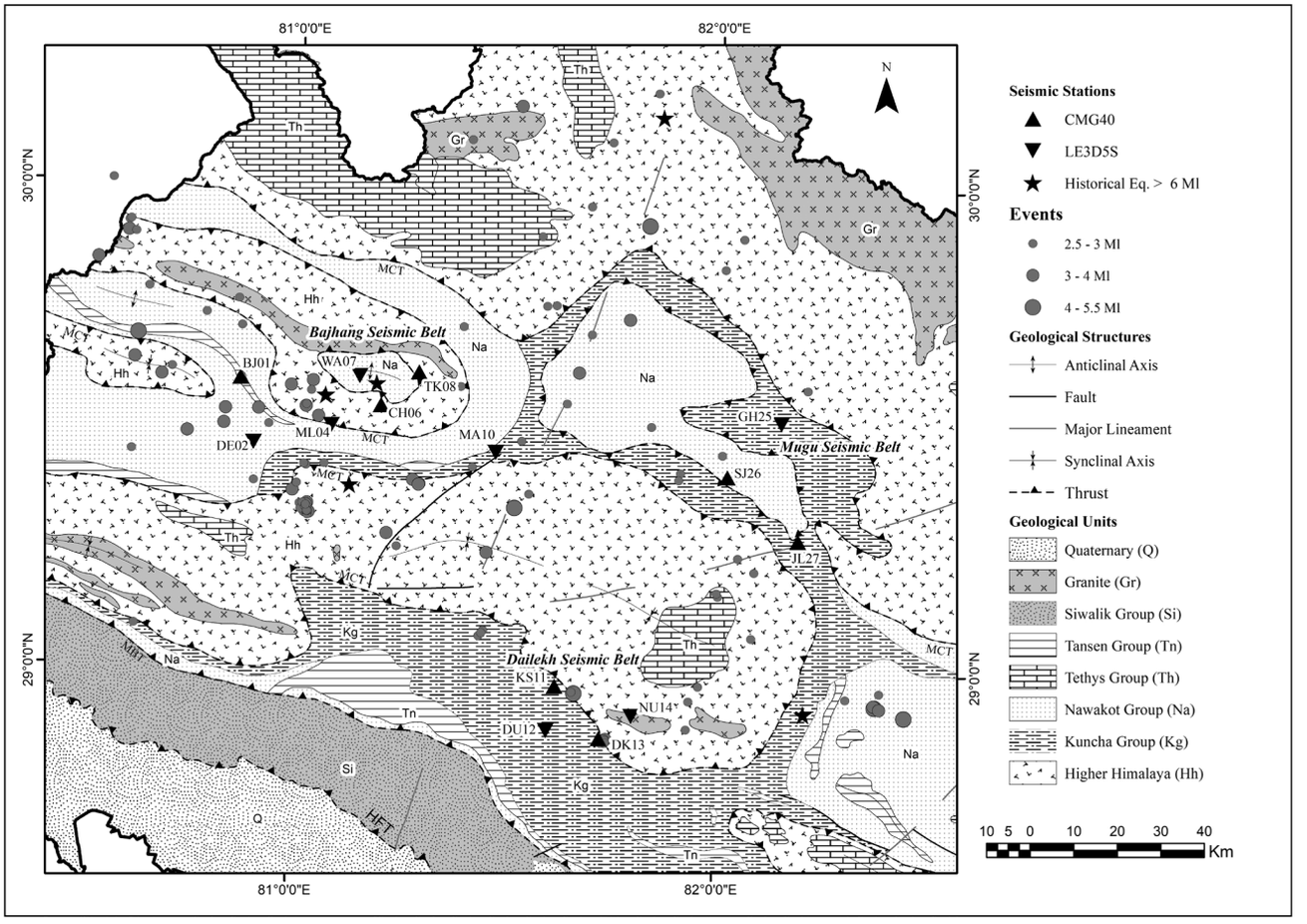

Fig. 1: Generalized geological map modified after DMG (2000) with earthquake location and seismic stations. Black triangles and inverted triangles represent the seismic stations. The size of black circles represents the magnitude of the events. Major tectonic divisions with generalized geological units and major thrusts are present as in legend.

the most widely used technique (e.g. Havskov et al., 1989; Kanao and Ito, 1991; Kosuga, 1992; Canas et al., 1995; Gupta et al., 1995; Kumar et al., 2005; Mukhopadhyay and Tyagi, 2007; Singh et al., 2012; Tripathi et al., 2012; Naghavi et al., 2017; Kandel et al., 2020) for estimating coda wave attenuation due to its simplicity, practicality, and effectiveness. It provides reliable estimates with moderate data requirements and low computational costs.

Single Back-scattering Model

The single back-scattering method of Aki and Chouet (1975) is a globally used method for local earthquakes. This model is based on the interaction of seismic waves with a single interface in a layered medium. From this model, coda wave amplitude, $A(f,t)$ for central frequency 'f' as follows (Aki, 1980).

$$A(f,t) = S(f)t^{-\alpha}\, exp\frac{-\pi f t}{Q_c} \qquad (1)$$

where *S (f)* represents the source function at central frequency 'f', over a narrow bandwidth signal, 't' is the lapse time measured from earthquake origin time,'α' geometrical spreading factor taken as unity for body wave and Q_c is the quality factor representing the average attenuation (Intrinsic and scattering attenuation) characteristic of the media. The simplest form after logarithm of Eq. (1) is given in the following form.

$$ln[A(f,t)] + \alpha \ln(t) = ln[S(f)] - \frac{\pi f t}{Q_c} \qquad (2)$$

This equation represents the equation of the straight line in which *[S(f)]* is a constant and the value of 'α' is unity. Then Eq. (2) becomes,

$$ln[A(f,t)t] = C - \left(\frac{\pi f}{Q_c}\right) t \qquad (3)$$

From Eq. (3), b = – πf / Qc is the slope of the straight line, and C is constant. So, the can be obtained from linear regression analysis between *In [A(f,t)t]* lapse time for each central frequency.

Data Analysis

The program 'CodaQ' prepared by Kumar et al. (2015), is used to estimate the attenuation characteristic of coda waves which is based on the single back-scattering model of Aki and Chouet (1975) and includes guidelines followed by SEISAN, EQK_SRC_PARA software (Ottermoller et al., 2021). The program 'CodaQ' requires Sesame Ascii File (SAF) format time series

data for input data. Selected seismograms are converted to SAF format by using the 'seisaf' sub-routine program of SEISAN (Ottermoller et al., 2021) before running the CodaQ. Then each seismogram is filtered at eight different frequencies (Table 1) using the Butterworth bandpass 4-th order filter (Fig. 2a). Signal to noise ratio is calculated for each central frequency for every record separately. The last 5 seconds of the selected coda window for each central frequency is selected for accounting for the signal-to-noise ratio (SNR).

We selected 30 s coda window length (Ottermoller et al., 2021) for all filtered seismograms which start from $2t_s$ (twice of direct S-wave arrival) to eliminate contamination caused by direct S-wave (Rautian and Khalturin, 1978) (Fig. 2b). After marking the P-wave and S-wave arrival time individually on waveforms, the Program automatically calculates the original times of each event using the relation, original time $=\{t_p\text{-}1.38\ (t_s\text{-}t_p)\}$ Continuously, each filtered seismogram is selected from coda arrival (TC) to coda arrival plus coda window length (30 s), and amplitude is multiplied by $t^{-\alpha}$ to account for geometrical attenuation (Fig. 2b). Fig. 2c represents the slope of the fitted straight line after plotting *ln [A(f,t)t]* versus lapse time. This fitted straight gives the value of coda Q of each waveform (Fig. 2c). The estimated Q_c at eight different central frequencies (Table 1) at 30 s coda windows length was filtered out with a signal-to-noise ratio of less than 2 and a correlation coefficient of less than 60%. The remaining Q_c are plotted as a function of frequency, according to the power relation $Q_c(f) = Q_0 f^n$ at each seismic station shown in Table 2, where Q_0 is Q_c at 1 Hz and f is the frequency and n represents the degree of frequency dependence.

RESULTS AND DISCUSSION

Estimation of Q_c

The estimated Q_0 (quality factor at 1 Hz) values of fourteen different stations (Table 2) range from 68.3 at the BJ01 station to 122.7 at the KS11 station. The value of Q_o increases with a decrease in frequency-dependent (n) at 30 s coda window length for all frequency bands as shown in Table 2. The values Q_c of BJ01, DE02, ML04, NU14, and WA07 seismic stations are relatively low as compared to DK13, KS11, and SJ26 seismic stations; however, all the seismic stations were installed on Lesser and Higher Himalaya, between MBT and MCT (Fig. 1). The value of n also varies from 0.96 at KS11 to 1.15 at BJ01. The mean Q_c values of this region at 30 s coda window length are calculated by averaging the Q_c of all stations. We obtained the mean value of Q_c is $(91.8 \pm 7.3) f^{1.07 \pm 0.03}$ is at 30 s coda window.

The effect of multiple scattering becomes insignificant for local events with a coda window of less than 100 s (Gao et al., 1983). As in this analysis, we have chosen a 30 s coda window length errors arising from multiple scattering should be insignificant. Similarly, the starting time of the coda wave for the coda window has been taken twice the S-wave travel time to avoid all direct waves (Rautian and Khalturin, 1978). The Q_o has a strong physical relationship with the wave propagating medium and is inversely proportional to the degree of medium heterogeneities (Aki, 1980; Paul et al., 2003; Mukhopadhyay

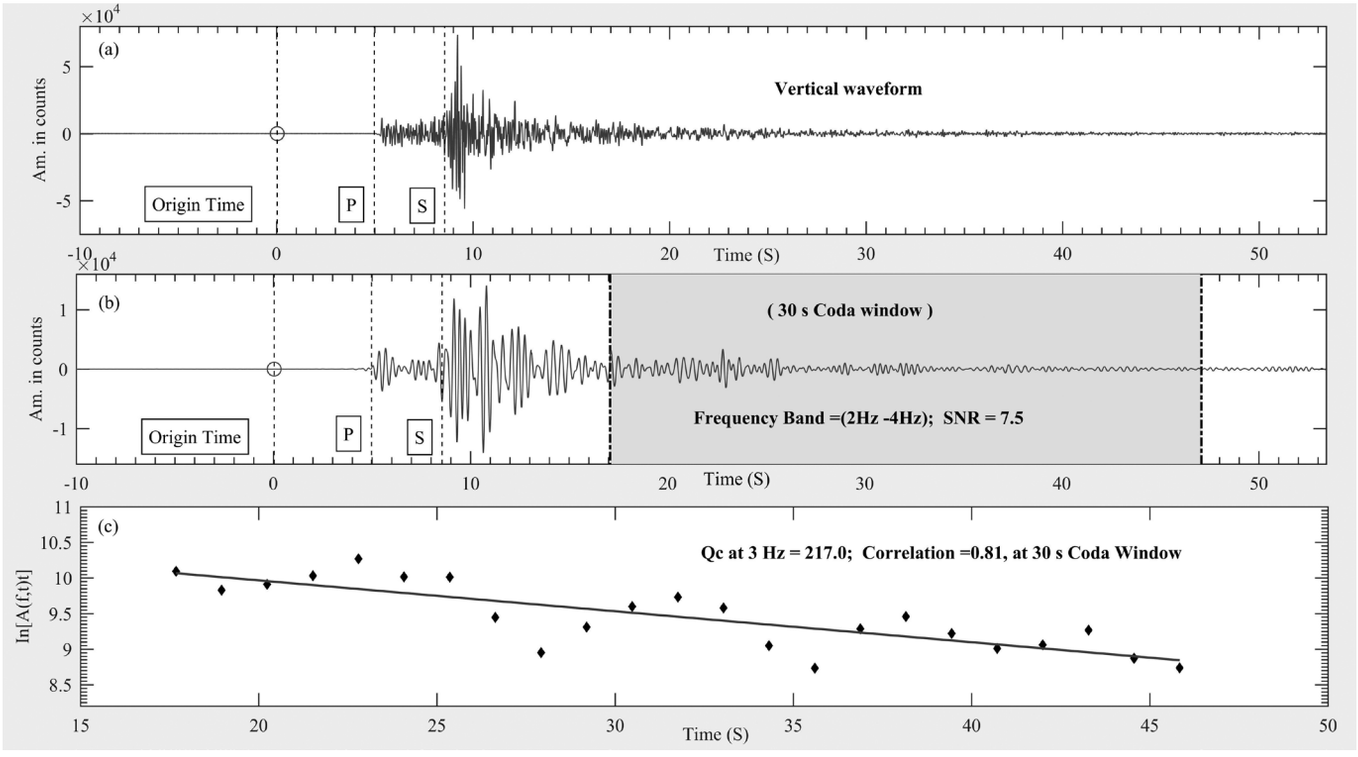

Fig. 2: Example of event processed. (a) the high-frequency vertical component waveform at ML04 seismic station on 13/12/2014, (b) Bandpass filtered waveform with 30 s coda window length at 2-4 Hz frequency band, and (c) The RMS amplitude (plotting *ln [A(f,t)t]* versus lapse time) values multiplied with lapse time window at central frequency 3 Hz. The slope of this fitting line is the value of Q_c at a given central frequency. P and S represent the P-wave and S-wave arrival time.

and Tyagi, 2007; Gupta et al., 2012). Therefore, the estimated low value of Q_o in this study indicates the presence of higher heterogeneities in the medium. On the other hand, for the seismically active regions, the values of *n* have been reported to vary from 0.70 to 1.10 (Roecker et al., 1982; Hellweg et al., 1995; Gupta et al., 1995; Gupta et al., 2012). The obtained values (from 0.96 to 1.15) of *n* represent the higher tectonic activities of the region (Aki, 1980; Roecker et al., 1982; Paul et al., 2003). Therefore Q_o and *n* results suggest the study area to be highly heterogeneous and seismo-tectonically active.

Spatial Variation of Q_o

The entire study area was divided into three seismic belts: Dailekh, Mugu and Bajhang seismic belts to compare the spatial variation of Q_c, based on the cluster of seismic events and variation of geological structures (Fig. 1 and Fig. 3). The value of Q_o of the Bajhang seismic belt (denser microseismicity of this area) is relatively low (84.5) and the value of frequency-dependent (*n*) at 30s coda window length is slightly high (1.08) as compared to seismic belts eastwards (Table 3). The concept of higher medium heterogeneities, lower the Q_o (Aki, 1980; Paul et al., 2003; Mukhopadhyay and Tyagi, 2007) validates the presence of complex geological structures and varied lithologies with multiple thrusts and fold belts in forming the Dadeldhura Klippe and Karnali Klippe (Dhital, 2015) within the region.

The Bajhang area has slightly more attenuation as compared to Mugu and Dailekh seismic belts. The values Q_c of both the Mugu and Dailekh seismic belts (eastern part of the study area) are almost identical. The spatial variation of the Q_o shows a decreasing trend towards the west as compared to eastern seismic belts (Fig. 3), which may linked to the microseismicity of the area (Jin and Aki, 1988; Singh et al., 2019). This westward decrease in Q_o is compatible with the previous works showing more dense microseismicity and more moderate earthquakes (6.0 – 7.0 Ml) in the Bajhang seismic belt than Mugu and Dailekh (Pandey et al., 1999). The variation of seismicity of this area is partially controlled by the geological structures, segmentation of the thrust and wider duplex (Pandey et al., 1999; Hoste-colomer et al., 2018; Laporte et al., 2021). The low Q_o region coincides with the high seismicity region revealing the weak zones forming potential for future ruptures (Jin and Aki, 1988; Singh et al., 2019). So the spatial variation of the Q_o values obtained in this study is directly related to the change in geological structure as we move westward.

Comparison with Other Studies

Each station of our study exhibits relatively low values of quality factor (Q_c) and high *n* values. The estimated values of the Q_c in this study are compared with those obtained from other tectonically active and stable regions of the world (Table 4, Fig. 4 and 5). Fig. 4 shows the graphic representations of frequency-dependent relation Q_c of different tectonically active Himalayan regions, including Nepal and Fig. 5 shows the other active regions in the world. The estimated Q_c is a combination of two intrinsic and scattering quality factors, which serve as the signature of the tectonic settings. For example: Intrinsic attenuation is higher than scattering in oceanic lithosphere ridges, and around the geothermal activity (Havskov et al., 1989; Yavuz and Baris, 2019) as compared to the Himalayan fold and thrust belt regions where more scattering is present than intrinsic (Aki, 1980).

The mean Q_c value in this study is greater as compared to Eastern Cuba (Biescas et al., 2007), Washington State (Havskov et al., 1989), Turkey (Yavuz and Baris, 2019), Friuli, Italy (Rovelli, 1982) and Southern Arabian Shield (Qaysi et

Table 2: Frequency-dependent relation of Q_c at each seismic station at 30 sec lapse time window.

Station Name	Q_c at 30 s coda window length	No of seismograms
BJ01	$68.3 \pm 9.1f^{1.15\pm0.05}$	57
CH06	$90.7 \pm 16.0f^{1.05\pm0.06}$	53
DE02	$78.3 \pm 8.9f^{1.09\pm0.04}$	77
DK13	$105.5 \pm 14.2f^{1.05\pm0.05}$	66
DU12	$86.1 \pm 5.7f^{1.11\pm0.02}$	67
GH25	$98.2 \pm 10.7f^{1.06\pm0.04}$	27
JL27	$98.8 \pm 17.3f^{1.07\pm0.06}$	48
KS11	$122.7 \pm 20.9f^{0.96\pm0.06}$	70
MA10	$96.2 \pm 12.3f^{1.07\pm0.05}$	61
ML04	$83.5 \pm 8.1f^{1.04\pm0.03}$	48
NU14	$83.7 \pm 9.3f^{1.09\pm0.04}$	68
SJ26	$102.5 \pm 16.3f^{1.03\pm0.06}$	41
TK08	$92.1 \pm 9.4f^{1.07\pm0.04}$	71
WA07	$83.8 \pm 10.7f^{1.09\pm0.05}$	51
Average, Q_c	$91.8 \pm 7.3f^{1.07\pm0.03}$	805

Table 3: Frequency-dependent relation of Q_c at three different seismic belts at 30 sec lapse time window.

Seismic Belts	Q_c at 30 s	Numbers of stations	No. of seismograms
Dailekh Belt	$98.9 \pm 8.7f^{1.05\pm0.03}$	4	271
Mugu Belt	$99.7 \pm 8.7f^{1.05\pm0.03}$	3	116
Bajhang Belt	$84.5 \pm 7.1f^{1.08\pm0.03}$	7	418
Average, Q_c	$91.8 \pm 7.3f^{1.07\pm0.03}$	Total = 14	Total = 805

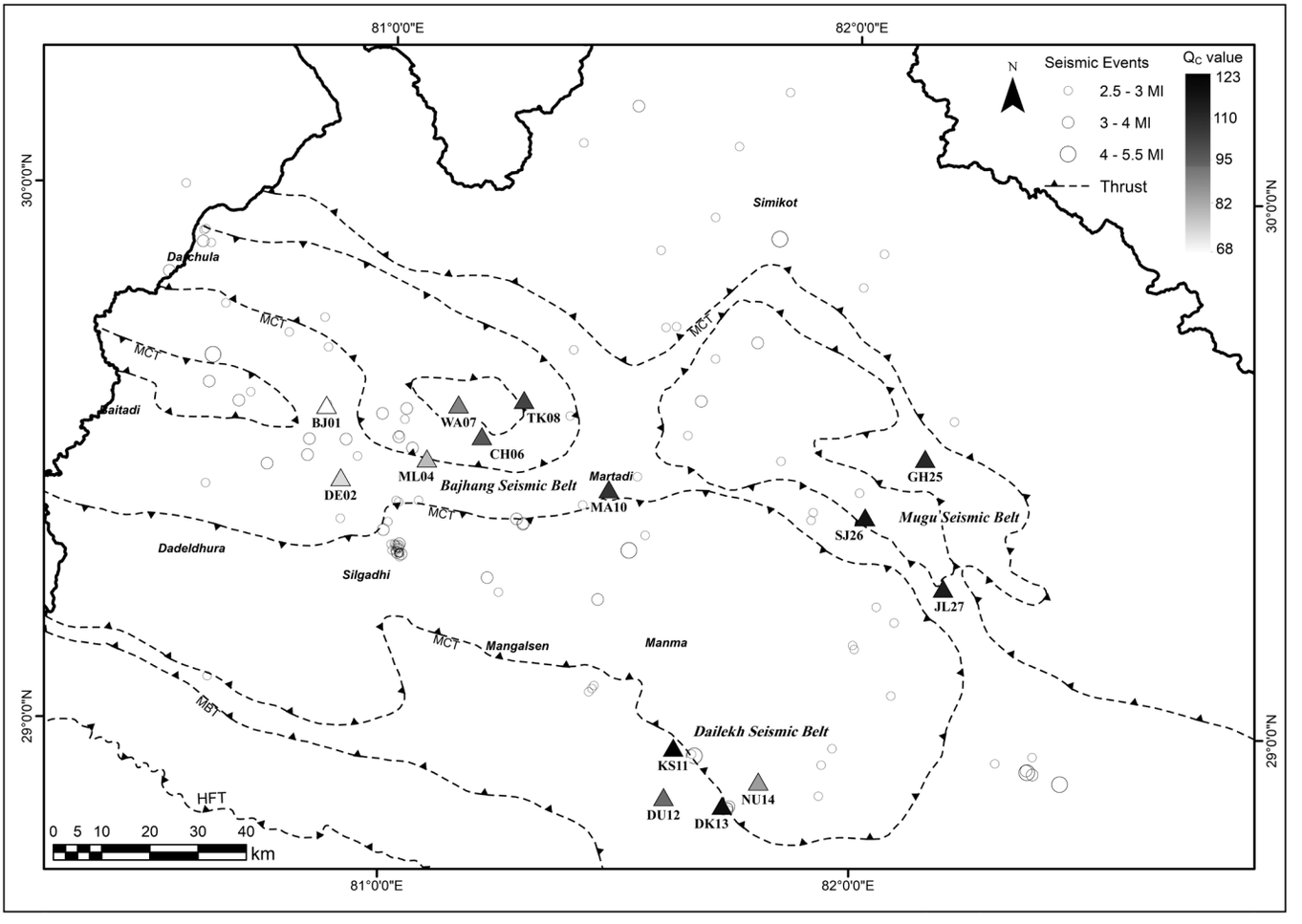

Fig. 3: Spatial distribution of Q_o at each seismic station at 30 s coda window. The MFT, MBT, and MCT are the major fault systems in this region. The colour code of triangles represents the seismic stations with the value of the quality factor.

al., 2022). Washington State and Turkey had more intrinsic attenuation due to thermal activities. The Q_c value of Midland Gujarat (Gupta et al., 2012), Kumaon Himalaya (Paul et al., 2003), and Northern Morocco (Boulanouar et al., 2017) is almost similar to our present study indicating almost similar attenuation characteristics and both Gujarat and Kumaon Himalaya lie on the same Himalaya range. Most of the events are concerned around the vicinity of the well-known MBT and MCT discontinuities in our study. The estimated Q_c value in this study is less than as compared to the previous study of South Central Alaska (Dutta et al., 2004), Garhwal Himalaya (Gupta et al., 1995), South Spain (Ibanez et al., 1990), Central region of Nepal (Kandel et al., 2020), Norway (Kvamme and Havskov, 1989), Western Nagao, Japan (Kosuga, 1992) Northwestern Himalaya, India (Kumar et al., 2005), Delhi region (Mohanty et al., 2009), Garhwal-Kumaon Himalaya (Mukhopadhyay and Sharma, 2010), Koyna region (Sharma et al., 2007), and Junagarh Gujarat (Sharma et al., 2011) (Table 4). Based on the difference in Q_o the study area is slightly more attenuated, as compared to central Nepal (Kandel et al., 2020) which might be attributed to geological structures and varied lithologies.

All the above-mentioned regions are tectonically active and have $Q_o < 200$, while Q_o values of seismo-tectonically stable regions such as Eastern North America (Atkinson and Boore,

Table 4: Frequency-dependent Q_c relationship for some tectonically active and stable regions of the world.

Region	Relation	Reference
Mid and Far-Western Nepal	$92f^{1.07}$	(Present study)
Eastern North American	$680f^{0.36}$	Atkinson and Boore (1995)
Eastern Cuba	$64f^{0.84}$	Biescas et al. (2007)
Northern Morocco	$97.58f^{0.96}$	Boulanouar et al. (2017)
South Central Alaska	$152f^{0.82}$	Dutta et al. (2004)
Garhwal Himalaya (India)	$125f^{0.95}$	Gupta et al. (1995)
Midland Gujarat (India)	$87f^{1.01}$	Gupta et al. (2012)
Washington State (USA)	$63f^{0.97}$	Havskov et al. (1989)
South Spain	$155f^{1.05}$	Ibanez et al. (1990)
Central region (Nepal)	$110f^{1.03}$	Kandel et al. (2020)
Norway	$120f^{1.09}$	Kavamme and Havskov (1989)
Western Nagao, Japan	$112f^{0.67}$	Kosuga (1992)
Northwestern Himalaya, India	$158f^{1.05}$	Kumar et al. (2005)
Delhi region (India)	$142f^{1.04}$	Mohanty et al. (2009)
Garhwal-Kumaon Himalaya	$119f0.99$	Mukhopadhyay and Sharma (2010)
Kumaon Himalaya (India)	$92f^{1.07}$	Paul et al. (2003)
New England	$460f^{0.4}$	Pulli (1984)
Southern Arabian Shield	$63f^{0.86}$	Qaysi et al. (2022)
Friuli, Italy	$80f^{1.1}$	Rovelli (1982)
Central Asia	$249f^{0.658}$	Sedaghati et. al (2019)
Koyna region, India	$117f^{0.97}$	Sharma et al. (2007)
Junagarh, Gujarat (India)	$170f^{0.97}$	Sharma et al. (2011)
Jamnagar Gujarat (India)	$224f^{0.98}$	Sharma et al. (2011)
Turkey	$77f^{0.8}$	Yavuz and Batis (2019)

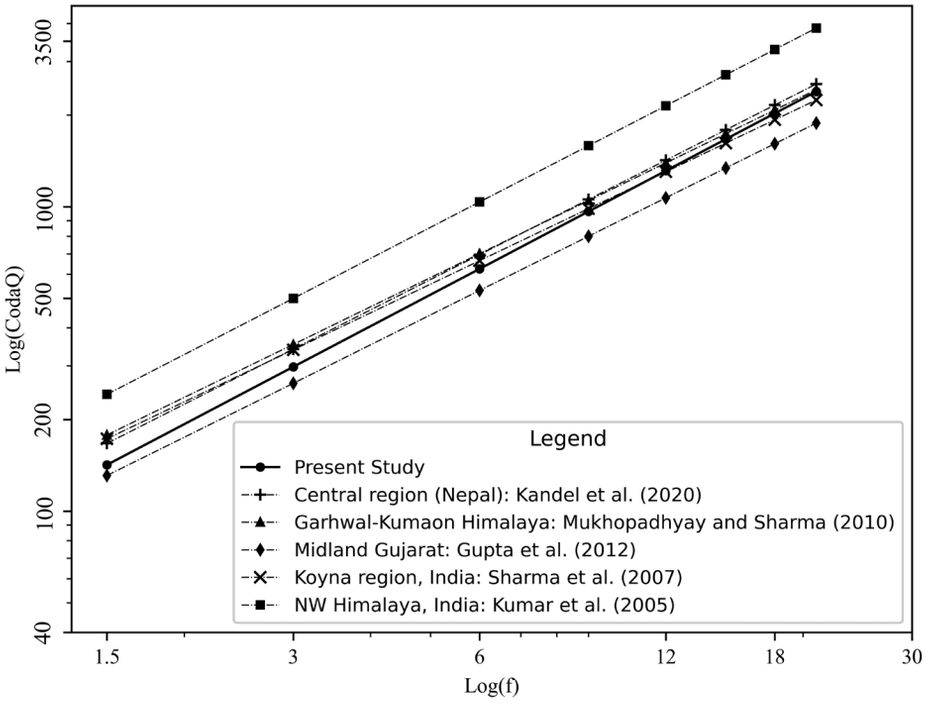

Fig. 4: Comparison of Q_c values for the Mid and Far-Western region of Nepal Himalaya, with some active Himalaya regions near the target of this study.

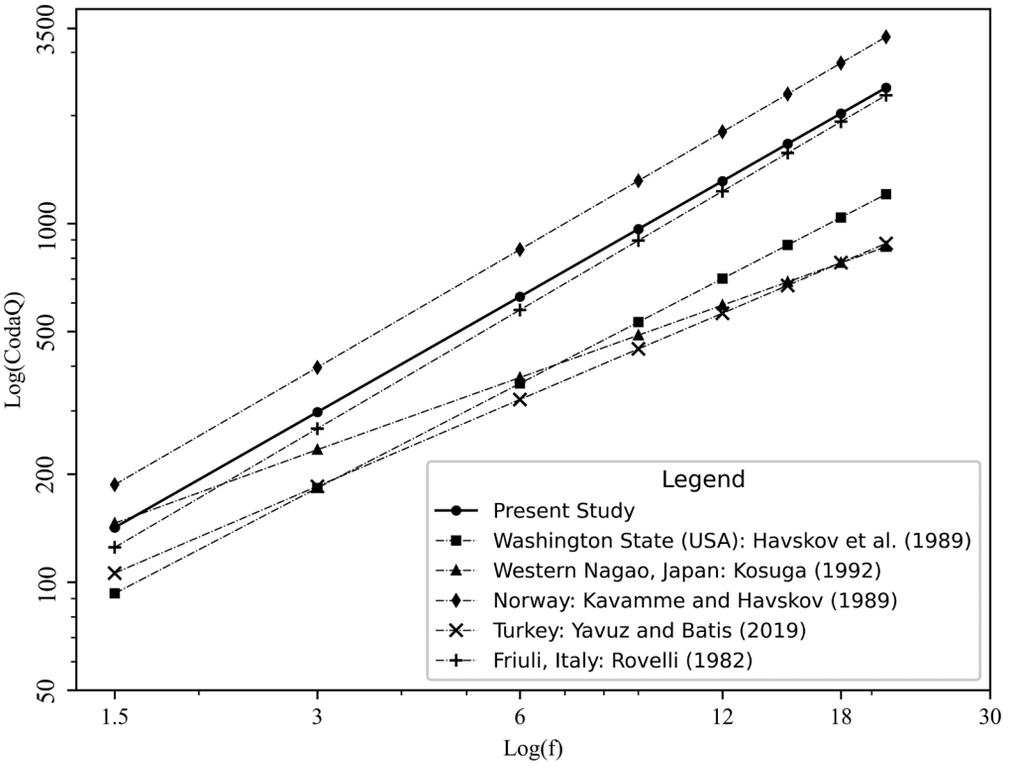

Fig. 5: Comparison of Q_c values for the Mid and Far-Western region of Nepal Himalaya, with some active regions of the world.

1995), New England (Pulli, 1984), Central Asia (Sedaghati et al., 2019), and Jamnagar Gujarat (Sharma et al., 2011) are relatively larger and *n* value relatively smaller (Table 4). Therefore, the Q_o and *n* obtained in this study are compatible with the results having similar tectonic settings of the other active regions of the world (Table 4).

CONCLUSIONS

High-frequency attenuation characteristic of the Mid and Far-Western region of Nepal Himalaya is described with the help of coda wave through a single back-scattering model. The quality factor (Q_c) of each seismic station was estimated in the form of a frequency-dependent (from 1.5 to 21 Hz) relation. We obtained the mean value of (Q_c) is (91.8±7.3) $f^{(1.07\pm0.03)}$ at 30 s coda window. The estimated mean Q_o and *n* values indicate that the medium (upper lithosphere) of the Mid and Far-Western region of Nepal Himalaya (the study area) is highly heterogeneous and seismo-tectonically active. The values of Q_o and *n* obtained at 30 s coda window from this study are compatible with the results obtained in having a similar tectonic setting in the adjoining regions. The estimated frequency-dependent relations are useful for earthquake source parameters and the modelling of strong ground motions.

ACKNOWLEDGMENTS

The temporal seismic network, HiKNet, was deployed in Far western Nepal, in which instruments belong to the French national pool of portable seismic instruments SISMOB-RESIF (INSU-CNRS) and was supported by the ANR-BHUTANEPAL (Grant ANR-13BS06-006-01). The authors are grateful to all researchers and supporting organizations for deploying and operating this temporary seismic network in Nepal.

REFERENCES

Aki, K., 1980, Attenuation of shear-waves in the lithosphere for frequencies from 0.05 to 25 Hz. Phys. Earth Planet. Inter. v. 21, pp. 50–60. https://doi.org/10.1016/0031-9201(80)90019-9

Aki, K., 1969, Analysis of the Seismic Coda of Local Earthquakes as Scattered Waves. J. Geophys. Res. v. 74, pp. 615–631.

Aki, K. and Chouet, B., 1975, Origin of coda waves: Source, attenuation, and scattering effects. J. Geophys. Res. v. 80, pp. 3322–3342. https://doi.org/10.1029/JB080i023p03322

Atkinson, G.M. and Boore, D.M., 1995, Ground-motion relations for eastern North America. Bull. Seismol. Soc. Am. v. 85, pp. 17–30.

Biescas, B., Rivera, Z. and Zapata, J.A., 2007, Seismic attenuation of coda waves in the eastern region of Cuba. Tectonophysics v. 429, pp. 99–109. https://doi.org/10.1016/j.tecto.2006.09.013

Bilham, R., 1995, Location and Magnitude of the 1833 Nepal Earthquake and Its Relation to the Rupture Zones of Contiguous Great Himalayan Earthquakes. Curr. Sci. v. 69, pp. 101–128.

Bollinger, L. and Lyon-Caen, H., RESIF, 2011, HiK-NET temporary experiment (RESIF-SISMOB). RESIF - Réseau Sismol. géodésique Français. https://doi.org/10.15778/resif.zo2014

Boulanouar, A., Moudnib, L. El, Padhy, S., Harnafi, M., Villaseñor, A., Gallart, J., Pazos, A., Rahmouni, A., Boukalouch, M. and Sebbani, J., 2017, Estimation of Coda Wave Attenuation in Northern Morocco. Pure Appl. Geophys. v. 175, pp. 883–897. https://doi.org/10.1007/s00024-017-1726-4

Canas, J.A., Pujades, L.G., Blanco, M.J., Soler, V. and Carracedo, J.C., 1995, Coda-Q distribution in the Canary Islands. Tectonophysics v. 246, pp. 245–261.

Cattin, R. and Avouac, J.P., 2000. Modelling mountain building and the seismic cycle in the Himalaya of Nepal. J. Geophys. Res. Solid Earth v. 105, pp. 13389–13407. https://doi.org/10.1029/2000jb900032

Dainty, A.M., 1981, A Scattering model to explain seismic Q observations in the lithosphere between 1 and 30 Hz. Geophys. Res. Lett. v. 8, pp. 1126–1128.

Dhital, M.R., 2015, Geology of the Nepal Himalaya, Regional Perspective of the Classic Collided Orogen, Regional Geology Reviews.

DMG, 2020, Geological map of Karnali and Sudurpaschim province, Nepal. Dep. Mines Geol.

Dutta, U., Biswas, N.N., Adams, D.A. and Papageorgiou, A., 2004, Analysis of S-wave attenuation in south-central Alaska. Bull. Seismol. Soc. Am. v. 94, pp. 16–28. https://doi.org/10.1785/0120030072

Gao, L.S., Lee, L.C., Biswas, N.N. and Aki, K., 1983, Comparison of the effects between single and multiple scattering on coda waves for local earthquakes. Bull. Seismol. Soc. Am. v. 73, pp. 377–389. https://doi.org/10.1785/BSSA0730020377

Goldstein, P. and Snoke, A., 2005, SAC availability for the IRIS community. Inc. Res. Institutions Seismol. Newsl.

Gupta, A.K., Sutar, A.K., Chopra, S., Kumar, S. and Rastogi, B.K., 2012, Attenuation characteristics of coda waves in Mainland Gujarat (India). Tectonophysics. https://doi.org/10.1016/j.tecto.2012.01.002

Gupta, S.C., Singh, V.N. and Kumar, A., 1995. Attenuation of coda waves in the Garhwal Himalaya, India. Phys. Earth Planet. Inter. v. 87, pp. 247–253.

Havskov, J., Malone, S., MeClorg, D. and Crosson, R., 1989, Coda Q for the State of Washington. Bull. Seismol. Soc. Am. v. 79, pp. 1024–1032.

Havskov, J. and Ottemoller, L., 2010, Routine data processing in earthquake seismology: With sample data, exercises and software. Springer Science and Business Media. https://doi.org/10.1007/978-90-481-8697-6

Hellweg, M., Spudich, P., Fletcher, J.B. and Baker, L.M., 1995, Stability of coda Q in the region of Parkfield, California: view from the US Geological Survey Parkfield dense seismograph array. J. Geophys. Res. 100, 2089–2102. https://doi.org/10.1029/94JB02888

Hossler, T., Bollinger, L., Sapkota, S.N., Lavé, J., Gupta, R.M. and Kandel, T.P., 2016, Surface ruptures of large Himalayan earthquakes in Western Nepal : Evidence along a reactivated strand of the Main Boundary Thrust. Earth Planet. Sci. Lett. 434, pp. 187–196. https://doi.org/10.1016/j.epsl.2015.11.042

Hoste-colomer, R., Bollinger, L., Lyon-caen, H., Adhikari, L.B., Baillard, C., Benoit, A., Bhattarai, M., Gupta, R.M., Jacques, E., Kandel, T.P., Koirala, B.P., Letort, J., Maharjan, K., Matrau, R., Pandey, R. and Timsina, C., 2018, Lateral variations of the midcrustal seismicity in western Nepal : Seismotectonic implications. Earth Planet. Sci. Lett. v. 504, pp. 115–125. https://doi.org/10.1016/j.epsl.2018.09.041

Ibanez, J.M., Pezzo, E. Del, Miguel, F. De, Herraiz, M., Alguacil, G., and Morales, J., 1990, Depth-dependent seismic attenuation in the Granada zone (Southern Spain). Bull. Seismol. Soc. Am. v. 80, pp. 1232–1244. https://doi.org/10.1785/BSSA0800051232

Jin, A. and Aki, K., 1988, Spatial and temporal correlation between coda Q and seismicity in China. Bull. Seismol. Soc. Am. v. 78, pp. 741–769.

Kanao, M. and Ito, K., 1991, Attenuation of S Waves and Coda Waves in the Inner Zone of Southwestern Japan. Bull. Disas. Prey. Res. Inst., Kyoto Univ. v. 41, pp. 87–107.

Kandel, T.P., Yamada, M. and Pokhrel, P., 2020, Determination of high-frequency attenuation characteristic of coda waves in the central region of Nepal Himalaya. J. Nepal Geol. Soc. v. 60, pp. 75–86.

Kosuga, M., 1992. Dependence of Coda Q on Frequency and Lapse Time in the Western Nagano Region, Central Japan. J. Phys. Earth v. 40, pp. 421–445. https://doi.org/10.4294/jpe1952.40.421

Kumar, A., Kumar, R., Ghangas, V. and Sharma, B., 2015, MATLAB codes (CodaQ) for estimation of attenuation characteristics of coda waves. Int. J. Adv. Res. J. www . journalijar . com Int. J. Adv. Res. v. 3, pp. 1078–1083.

Kumar, N., Parvez, I.A. and Virk, H.S., 2005. Estimation of coda wave attenuation for NW Himalayan region using local earthquakes. Phys. Earth Planet. Inter. v. 151, pp. 243–258. https://doi.org/10.1016/j.pepi.2005.03.010

Kvamme, L. and Havskov, J., 1989, Q in southern Norway. Bull. Seismol. Soc. Am. v. 79, pp. 1575–1588.

Laporte, M., Bollinger, L., Duverger, C., Letort, J., Riesner, M., Koirala, B.P., Bhattarai, M., Kandel, T., Timsina, C. and Adhikari, L.B., 2021. Seismicity in far western Nepal reveals flats and ramps along the Main Himalayan Thrust. Geophys. J. Int. v. 226, pp. 1747–1763. https://doi.org/10.1093/gji/ggab159

Mohanty, W.K., Prakash, R., Suresh, G., Shukla, A.K., Yanger Walling, M. and Srivastava, J.P., 2009, Estimation of coda wave attenuation for the National Capital Region, Delhi, India using local earthquakes. Pure Appl. Geophys. v. 166, pp. 429–449. https://doi.org/10.1007/s00024-009-0448-7

Molnar, P. and Tapponnier, P., 1975, Cenozoic Tectonics of Asia: Effects of a continental Collision. Science v. (80), 189, pp. 419–426.

Mukhopadhyay, S. and Sharma, J., 2010, Attenuation characteristics of Garwhal–Kumaun Himalayas from analysis of coda of local earthquakes. J. Seismol. v. 14, pp. 693–713. https://doi.org/10.1007/s10950-010-9192-9

Mukhopadhyay, S. and Tyagi, C., 2007, Lapse time and frequency-dependent attenuation characteristics of coda waves in the Northwestern Himalayas. J. Seismol. v. 11, pp. 149–158. https://doi.org/10.1007/s10950-006-9042-y

Naghavi, M., Rahimi, H., Moradi, A. and Mukhopadhyay, S., 2017, Spatial variations of seismic attenuation in the North West of Iranian plateau from analysis of coda waves. Tectonophysics v. 708, pp. 70–80. https://doi.org/10.1016/j.tecto.2017.04.026

Ottermoller, L., Voss, P.H. and Havskov, J., 2021, SEISAN Earthquake Analysis Software for Windows, Solaris, Linux, and Macosx.

Pandey, M, Tandukar, R., Avouac, J., Vergne, J. and Héritier, T., 1999, Seismotectonics of the Nepal Himalaya from a local seismic network. J. Asian Earth Sci. v. 17, pp. 703–712. https://doi.org/10.1016/s1367-9120(99)00034-6

Pandey, M. R., Tandukar, R.P., Avouac, J.P., Vergne, J. and Héritier, T., 1999. Seismotectonics of the Nepal Himalaya from a local seismic network. J. Asian Earth Sci. v. 17, pp. 703–712. https://

doi.org/10.1016/S1367-9120(99)00034-6

Paul, A., Gupta, S.C. and Pant, C.C., 2003, CODA Q estimates for Kumaun Himalaya. Proc. Indian Acad. Sci. Earth Planet. Sci. v. 112, pp. 569–576. https://doi.org/10.1007/BF02709780

Pulli, J., 1984, Attenuation of coda waves in New England. Bull. Seismol. Soc. Am. v. 74, pp. 1149–1166.

Qaysi, S., Abdelfattah, A.K., Almadani, S., Olaniyan, A. and Alzahrani, H., 2022, Attenuation characteristics of coda wave in southern Arabian Shield. J. King Saud Univ. - Sci. v. 35, pp. 1–10. https://doi.org/10.1016/j.jksus.2022.102372

Rautian, T.G. and Khalturin, V.I., 1978, The use of the coda for determination of the earthquakes source spectrum. Bull. Seismol. Soc. Am. v. 68, pp. 923–948.

Riesner, M., Bollinger, L., Hubbard, J., Guérin, C., Lefèvre, M., Vallage, A., Shah, C.B., Kandel, T.P. and Haines, S., 2021, Localized extension in megathrust hanging wall following great earthquakes in western Nepal. Sci. Rep. v. 11, p. 21521. https://doi.org/10.1038/s41598-021-00297-4

Roecker, S.W., Tucker, B., King, J. and Hatzfeld, D., 1982, Estimates of Q in central Asia as a function of frequency and depth using the coda of locally recorded earthquakes. Bull. Seismol. Soc. Am. v. 72, pp. 129–149.

Rovelli, A., 1982, On the frequency dependence of Q in friuli from shortperiod digital records. Bull. Seismol. Soc. Am. 72, pp. 2369–2372.

Sato, H., 1977a, Energy propagation including scattering effects single isotropic scattering approximation. J. Phys. Earth v. 25, pp. 27–41. https://doi.org/10.4294/jpe1952.25.27

Sato, H., 1977b, Single isotropic scattering model including wave conversions simple theoretical model of the short period body wave propagation. J. Phys. Earth v. 25, pp. 163–176. https://doi.org/10.4294/jpe1952.25.163

Sato, H., Fehler, M.C., 1998. Seismic Wave Propagation and Scattering in the Heterogeneous Earth. American Inatitude of Physics. Press/Springer, New york, P. 308.

Sato, H., Fehler, M.C. and Maeda, T., 2012, Seismic Wave Propagation and Scattering in the Heterogenous Earth, second edi. ed. Springer.

Sedaghati, F., Nazemi, N., Pezeshk, S., Ansari, A., Daneshvaran, S. and Zare, M., 2019, Investigation of coda and body wave attenuation functions in Central Asia. J. Seism.

Sharma, B., Kumar, D., Teotia, S.S., Rastogi, B.K., Gupta, A.K., and Prajapati, S., 2011, Attenuation of coda waves in the Saurashtra region, Gujarat (India). Pure Appl. Geophys. pp. 89–100. https://doi.org/10.1007/s00024-011-0295-1

Sharma, B., Teotia, S.S. and Kumar, D., 2007, Attenuation of P, S, and coda waves in Koyna region, India. J. Seismol. v. 11, pp. 327–344. https://doi.org/10.1007/s10950-007-9057-z

Singh, C., Basha, S.K., Shekar, M. and Chadha, R.K., 2012, Spatial variation of coda wave attenuation in the Southern Indian Shield and its implications. Geol. Acta v. 10, pp. 309–318. https://doi.org/10.1344/105.000001751

Singh, C., Biswas, R., Jaiswal, N. and Ravi Kumar, M., 2019, Spatial variations of coda wave attenuation in Andaman–Nicobar subduction zone. Geophys. J. Int. v. 217, pp. 1515–1523. https://doi.org/10.1093/gji/ggz098

Stein, S. and Wysession, M., 2009, An Introduction to Seismology, Earthquakes, and Earth Structure. Wiley-Blackwell.

Stevens, V.L. and Avouac, J.P., 2015, Interseismic coupling on the main Himalayan thrust. Geophys. Res. Lett. v. 42, pp. 5828–5837. https://doi.org/10.1002/2015GL064845

Subedi, S., Hetényi, G., Vergne, J., Bollinger, L., Lyon-Caen, H., Farra, V., Adhikari, L.B. and Gupta, R.M., 2018, Imaging the Moho and the Main Himalayan Thrust in Western Nepal With Receiver Functions. Geophys. Res. Lett. v. 45, pp. 13,222-13,230. https://doi.org/10.1029/2018GL080911

Tabei, T., Ohzono, M., Silwal, B.R., Bhandari, R.P., Adhikari, L.B., Chand, J.B. and Kandel, T.P., 2024, Geodetic plate coupling and seismic potential on the main Himalayan thrust in Nepal. Earth, Planets Sp. online, pp. 1–13. https://doi.org/10.1186/S40623-024-02016-5

Tripathi, J.N., Singh, P. and Sharma, M.L., 2012, Variation of seismic coda wave attenuation in the Garhwal region, northwestern Himalaya. Pure Appl. Geophys. v. 169, pp. 71–88. https://doi.org/10.1007/s00024-011-0316-0

Yavuz, E. and Baris, S., 2019, Determination of coda wave attenuation characteristic of the Armutlu Peninsula and its surroundings (Middle Marmara region, Turkey). Ann. Geophysics 62. https://doi.org/10.4401/ag-7775